

Anisotropic field-induced ordering in the triangular-lattice quantum spin liquid NaYbSe₂

K. M. Ranjith ^{1,*} S. Luther,^{2,3} T. Reimann ² B. Schmidt ¹ Ph. Schlender ⁴ J. Sichelschmidt ¹ H. Yasuoka,¹
A. M. Strydom,⁵ Y. Skourski,² J. Wosnitzer,^{2,3} H. Kühne,² Th. Doert ⁴ and M. Baenitz^{1,†}

¹Max Planck Institute for Chemical Physics of Solids, 01187 Dresden, Germany

²Hochfeld-Magnetlabor Dresden (HLD-EMFL) and Würzburg-Dresden Cluster of Excellence *ct.qmat*,
Helmholtz-Zentrum Dresden-Rossendorf, 01328 Dresden, Germany

³Institut für Festkörper- und Materialphysik, TU Dresden, 01062 Dresden Germany

⁴Faculty of Chemistry and Food Chemistry, TU Dresden, 01062 Dresden, Germany

⁵Highly Correlated Matter Research Group, Department of Physics, University of Johannesburg, P.O. Box 524,
Auckland Park 2006, South Africa



(Received 2 October 2019; revised manuscript received 4 December 2019; published 19 December 2019)

High-quality single crystals of NaYbSe₂, which resembles a perfect triangular-lattice antiferromagnet without intrinsic disorder, are investigated by magnetization and specific heat, as well as the local probe techniques nuclear magnetic resonance (NMR) and electron spin resonance. The low-field measurements confirm the absence of any spin freezing or long-range magnetic order down to 50 mK, which suggests a quantum spin liquid ground (QSL) state with gapless excitations. Instability of the QSL state is observed upon applying magnetic fields. For the $H \perp c$ direction, a field-induced magnetic phase transition is observed above 2 T from the $C_p(T)$ data, agreeing with a clear $\frac{M_s}{3}$ plateau of $M(H)$, which is associated with an up-up-down spin arrangement. For the $H \parallel c$ direction, a field-induced transition could be evidenced at a much higher field range (9–21 T). The ²³Na NMR measurements provide microscopic evidence of field-induced ordering for both directions. A reentrant behavior of T_N , originating from the thermal and quantum spin fluctuations, is observed for both directions. The anisotropic exchange interactions $J_{\perp} \simeq 4.7$ K and $J_z \simeq 2.33$ K are extracted from the modified bond-dependent XXZ model for the spin- $\frac{1}{2}$ triangular-lattice antiferromagnet. The absence of magnetic long-range order at zero fields is assigned to the effect of strong bond frustration, arising from the complex spin-orbit entangled $4f$ ground state. Finally, we derive the highly anisotropic magnetic phase diagram, which is discussed in comparison with the existing theoretical models for spin- $\frac{1}{2}$ triangular-lattice antiferromagnets.

DOI: [10.1103/PhysRevB.100.224417](https://doi.org/10.1103/PhysRevB.100.224417)

I. INTRODUCTION

The search for a quantum spin liquid (QSL) state, a highly entangled state with fractionalized excitations, has been at the forefront of current condensed-matter physics research [1–3]. Spin- $\frac{1}{2}$ triangular-lattice antiferromagnets (TLAFs) with antiferromagnetic (AF) nearest-neighbor (NN) interactions are considered the prime candidate for this search, in which Anderson proposed a QSL ground state more than 40 years ago [4]. Even though the ground state of the Heisenberg TLAF model is now known to be a 120° AF ordered state [5,6], it can easily be perturbed by different mechanisms. For instance, the presence of a next-NN interaction [7,8], anisotropic planar NN exchange interactions [9], or spatially random exchange interactions (bond randomness) [10] may suppress the ordering and consequently stabilize the QSL ground states. Experimentally, several QSL candidate materials have since been reported, including κ -(BEDT-TTF)₂Cu₂(CN)₃, EtMe₃Sb[Pd(dmit)₂]₂, and Ba₃CuSb₂O₉ [11–17].

Rare-earth-based frustrated spin systems have recently attracted much attention [18,19]. The strong spin-orbit coupling

(SOC) associated with the rare-earth ion leads to highly anisotropic and bond-dependent exchange interactions between the moments and may host strong quantum fluctuations, which can play a crucial role in stabilizing the QSL state [20–23]. YbMgGaO₄, a $4f$ -based triangular-lattice system, has been investigated rigorously and proposed as a promising QSL candidate [24,25]. The absence of magnetic ordering down to 48 mK, an anomalous $C_v \propto T^{2/3}$ behavior [24], and the presence of an excitation continuum [26,27] are attributed to the QSL state with spinon excitations. On the other hand, the lack of a significant contribution from the magnetic excitations to the thermal conductivity [28], a persistent excitation continuum even in the high-field polarized phase [27], and the sizable broadening of crystal electric field (CEF) excitations [27,29] question the QSL ground state. The inherent structural disorder, a random distribution of Mg²⁺ and Ga³⁺ ions present in this system, mimics a spin-liquid-like state at low temperatures; instead, a robust collinear or stripe magnetic order is expected for a disorder-free version of YbMgGaO₄ theoretically [30].

On the other hand, theoretical studies propose a fascinating phase diagram for TLAFs in external magnetic fields [31–33]. Thermal and quantum spin fluctuations can favor different coplanar (an oblique version of the 120° state, Y phase, and 2:1 canted phase) and collinear [up-up-down (uud) phase]

*ranjith.kumar@cpfs.mpg.de

†michael.baenitz@cpfs.mpg.de

spin configurations. The stabilization of the collinear uud phase results in a $\frac{M_s}{3}$ plateau (M_s is the saturation magnetization) for a finite field range in the magnetization curve [31,32]. Experimentally, such a phase diagram has been observed in the spin- $\frac{1}{2}$ triangular-lattice compounds Cs_2CuBr_4 [34,35] and $\text{Ba}_3\text{CoSb}_2\text{O}_9$ [36,37].

The family of Yb dichalcogenide delafossites NaYbCh_2 ($Ch = \text{O}, \text{S}, \text{and Se}$) has recently been explored as a perfect spin- $\frac{1}{2}$ TLAF without inherent disorder [38–40]. Here, the combination of the SOC and the crystal electric field (CEF) leads to a Kramers doublet ground state for the Yb^{3+} ion, so that the low-temperature properties can be described by an effective spin- $\frac{1}{2}$ Hamiltonian. The energy gap between the ground state and the first excited doublet was found to be $\Delta/k_B \sim 200$ and ~ 400 K for NaYbS_2 [39] and NaYbO_2 [40,41], respectively, which suggests an effective spin- $\frac{1}{2}$ ground state. Experimentally, this is confirmed by specific heat measurements, which reveal a magnetic entropy of $R \ln(2)$ per Yb^{3+} ion [39,40]. Zero-field Muon-spin relaxation (μSR) and heat capacity measurements down to 50 mK confirmed the absence of magnetic long-range order (LRO), and suggested a QSL ground state with gapless excitations for NaYbS_2 and NaYbO_2 [39–41]. Furthermore, an excitation continuum with the spectral weight accumulating around the K point, which is expected for a QSL state, was observed in neutron studies of polycrystalline NaYbO_2 [41]. In NaYbO_2 , this QSL state is found to be suppressed by the application of external magnetic fields, and a field-induced ordered state was evidenced by magnetization, heat capacity, ^{23}Na nuclear magnetic resonance (NMR) [40], and neutron diffraction [42]. NaYbCh_2 compounds ($Ch = \text{O}, \text{S}, \text{and Se}$) provide a unique platform to study the field-induced crossover from an emerging spin-orbit-driven QSL at low fields to an isotropic two-dimensional (2D) planar spin- $\frac{1}{2}$ TLAF with particular types of LRO at much higher fields.

It should be mentioned that, in contrast to previous studies on NaYbO_2 [40–42], NaYbSe_2 is available in single-crystalline form, allowing for the determination of anisotropic static and dynamic magnetic properties. Here, we show that the emergent QSL ground state is associated with the quantum fluctuations and strong frustration, arising from the complex bond-dependent exchange interactions. The triangular arrangement of edge-shared YbSe_6 octahedra favors bond-dependent frustration. Each bond can be represented by an individual exchange matrix where the off-diagonal terms are responsible for the strong bond frustration. As these off-diagonal terms are usually small, they can be wiped out upon the application of external fields, converting the system into a more classical anisotropic planar spin- $\frac{1}{2}$ TLAF.

II. EXPERIMENT

Single crystals of NaYbSe_2 are synthesized by using NaCl , Yb metal grains, and Se as starting materials. All chemicals are stored and handled in an argon-filled glove box. For the syntheses of NaYbSe_2 , 825.5 mg (20 mmol, 20 equivalents) NaCl (lab stock, dried), 122.2 mg (0.71 mmol, 1 eq.) Yb (MaTeck, 99.92%, rod), and 133.9 mg (1.7 mmol, 2.4 eq.) Se (lab stock, sublimed) are mixed in a fused silica tube with an internal glassy carbon crucible. The tube is evacuated and

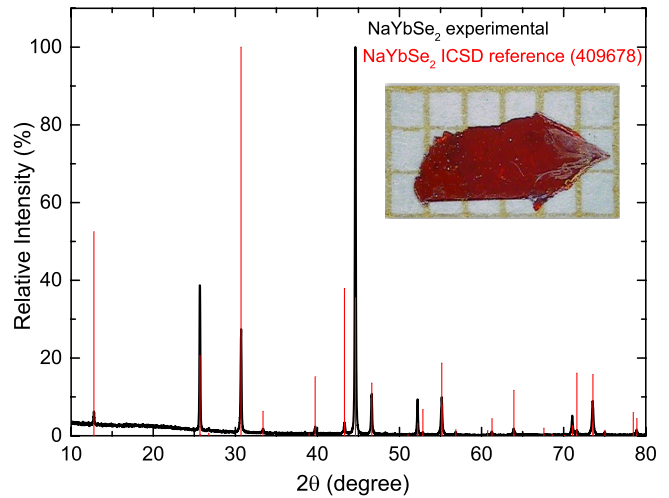


FIG. 1. Powder XRD pattern for a NaYbSe_2 sample compared with the ICSD reference (409678). Inset: Single crystal of NaYbSe_2 .

flame sealed, placed upright in a muffle furnace, and heated up to 400 °C at 180 K/h and equilibrated there for 2 h, before being heated to 850 °C at 20 K/h. After one week, the temperature is decreased 40 K/h to room temperature. After opening at ambient atmosphere, the sample is removed, and the alkali halide is rinsed off with water. The NaYbSe_2 crystals are washed several times with water and ethanol and dried in the hood. Polycrystalline samples of NaLuO_2 for comparison were synthesized by a solid-state reaction starting from Na_2O and Lu_2O_3 . The mixed powder was ground in a mortar under Ar atmosphere, placed in an alumina crucible, and heated up to 800 °C for 12 h in air. The material was then ground again and washed with distilled water and ethanol to remove the residual Na_2O . The phase purity of the samples was confirmed by powder x-ray diffraction (XRD) with a Stoe Stadi-P powder diffractometer using $\text{Cu } K\alpha$ radiation ($\lambda = 1.54056$ nm) and a Mythen 1K strip detector in flat-sample transmission mode (Fig. 1). In the diffraction pattern, all reflections can be assigned to the designated target phases; no reflections of by-products are observed. Due to the thin platelike shape of the crystals and the respective preferred orientation of the flakes, reflections with a major contribution of the Miller index l are highly overestimated.

Magnetization measurements were performed with a superconducting quantum interference device magnetometer [magnetic property measurement system (MPMS)] and a vibrating sample magnetometer. The MPMS with a ^3He insert was used for the low-temperature magnetization (down to 500 mK). The angular-resolved susceptibility measurements were performed using a commercial horizontal rotator from Quantum Design. Specific-heat measurements were conducted with a commercial physical property measurement system (Quantum Design) with a ^3He insert down to 350 mK on NaYbSe_2 single crystals and pressed pellets of NaLuO_2 powder samples. The specific heat down to 50 mK was obtained in a $^3\text{He}/^4\text{He}$ dilution fridge setup. The magnetization measurements in pulsed magnetic fields up to 35 T were performed at the Dresden High Magnetic Field Laboratory

(HLD) with a compensated pickup-coil system in a pulse field magnetometer in a home-built ^3He cryostat.

Electron spin resonance (ESR) experiments were carried out with a standard continuous-wave spectrometer. We measured the power P absorbed by the sample from a transverse magnetic microwave field (X band, $\nu = 9.4$ GHz) as a function of an external, static magnetic field $\mu_0 H = B$. In order to improve the signal-to-noise ratio, a lock-in technique was used, which yields the derivative of the resonance signal, dP/dH . NMR measurements were performed using Tecmag Apollo and Redstone spectrometers with a standard probe and a sweepable superconducting magnet. Field sweep NMR spectra were obtained by the integration of spin echo signals at a fixed frequency. The spectra at low temperatures were constructed from frequency-swept Fourier transform sums. Spin-lattice relaxation rates were measured using a standard inversion recovery method, where the nuclear magnetization $M(t)$ was obtained from the recovery of the spin-echo magnitude as a function of the time interval τ between the inversion pulse (π pulse) and the $\pi/2 - \pi$ spin-echo sequence.

III. RESULTS

A. Crystal structure and magnetic anisotropy

Single crystals of NaYbSe_2 with lateral crystallite size in the millimeter range were synthesized by flux reactions (see the Supplemental Material [43]). NaYbSe_2 has a delafossite-type structure with the $R\bar{3}m$ space group (No. 166). As shown in Fig. 2(a), the crystal structure is composed of edge-shared YbSe_6 and NaSe_6 octahedra. The YbSe_6 octahedra are weakly distorted with two large equilateral triangles with edge length $l \simeq 4.06$ Å and six small isosceles triangles with two edges of length $s \simeq 3.7$ Å and one edge of length l . The distorted octahedra are tilted along the Yb-Yb bond by an angle $\alpha = \cos^{-1}(l/\sqrt{3}s) \simeq 53.33^\circ$, such that the large triangular faces are perpendicular to the crystallographic c direction. The tilt of the YbSe_6 octahedra in NaYbSe_2 is smaller than that in NaYbO_2 ($\alpha \simeq 47.70^\circ$) and NaYbS_2 ($\alpha \simeq 48.60^\circ$) and the tilting angle $\alpha \sim 54.74^\circ$ for an undistorted octahedron. The NaSe_6 octahedra are distorted as well. The shortest Yb-Yb distances are found in the ab plane, forming triangular layers which are well separated by edge-shared NaSe_2 layers. A rhombohedral stacking (ABCA stacking) of magnetic Yb triangular layers provides additional strong frustration of the interlayer interactions.

Figure 2(c) shows the angle-resolved magnetic susceptibility $\chi(\theta)$ of a single crystal sample where the crystal was successively rotated from the ab plane ($\theta = 0^\circ$) to the c direction ($\theta = \pm 90^\circ$). The presence of well-defined minima and maxima clearly reveals the existence of a significant easy-plane-type anisotropy in NaYbSe_2 . The anisotropy of χ vanishes towards high temperatures. The susceptibility anisotropy of $\chi_\perp/\chi_\parallel \simeq 1.5$ for NaYbSe_2 at $T \simeq 20$ K is smaller than that of NaYbS_2 (~ 2) at the same temperature. Usually, the anisotropy in χ captures both spin and exchange anisotropy.

ESR provides direct information about the spin anisotropy. Figure 2(b) shows the ESR lines at 20 K for the field applied along the ab plane and c axis. The well-resolved and narrow ESR spectra obtained for NaYbSe_2 single crystals indicate the

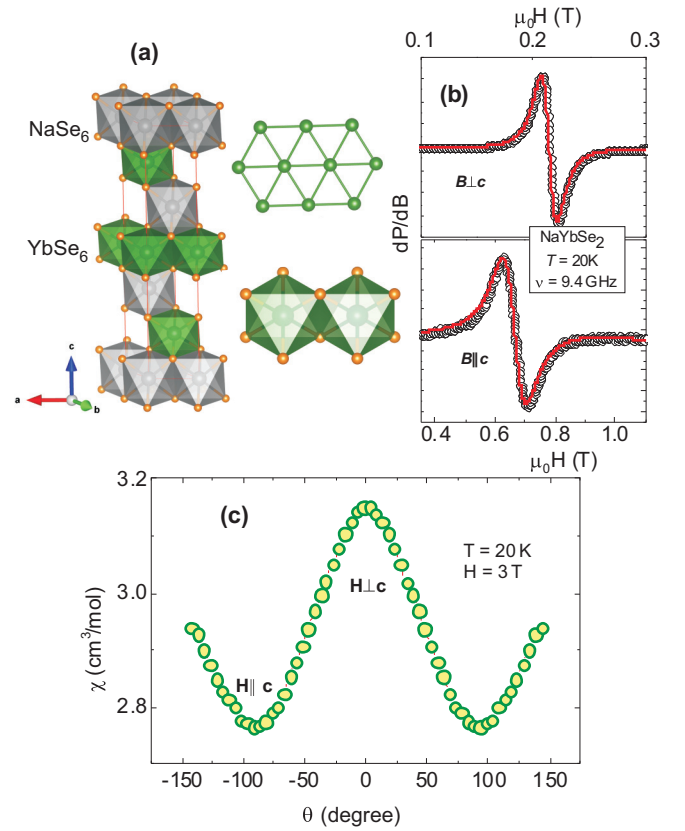


FIG. 2. (a) Schematic crystal structure of NaYbSe_2 . Yb triangular layers (green) are formed by edge-shared YbSe_6 octahedra in the ab plane. (b) ESR spectra measured at 20 K for both the $H \perp c$ and $H \parallel c$ directions. (c) Angular dependence of the magnetic susceptibility obtained at 3 T and 20 K for a NaYbSe_2 single crystal.

absence of intrinsic structural disorder. This is in contrast to the recently reported Yb-based QSL candidate YbMgGaO_4 , for which the structurally distorted occupancy of Ga and Mg leads to an off-center displacement of Yb^{3+} ions, resulting in a distribution of g values with rather broad ESR spectra. Furthermore, the ESR measurements for $H \perp c$ [Fig. 2(b), bottom panel] and $H \parallel c$ [Fig. 2(b) top panel] of NaYbSe_2 yield strongly anisotropic g values of $g_\perp = 3.13(4)$ and $g_\parallel = 1.01(1)$. The g -value anisotropy, which corresponds to the spin anisotropy, is obtained as $g_\perp/g_\parallel \simeq 3.1$, which is significantly smaller than that of NaYbS_2 ($g_\perp/g_\parallel \simeq 5.6$) [39,44]. Due to the lack of neutron scattering data, a first estimate of the energy gap Δ between the ground-state doublet and the first excited doublet could be obtained from the temperature dependence of the ESR line width, which increases exponentially towards high temperatures due to an Orbach process. The obtained value of $\Delta/k_B \sim 160 \pm 30$ K confirms the low-temperature pseudospin- $\frac{1}{2}$ ground state [45].

B. Low-field thermodynamics

1. Magnetic susceptibility

Figure 3(a) shows the temperature dependence of the magnetic susceptibility of NaYbSe_2 measured for fields applied in the ab plane, $\chi_\perp(T)$, and along the c axis, $\chi_\parallel(T)$. At higher

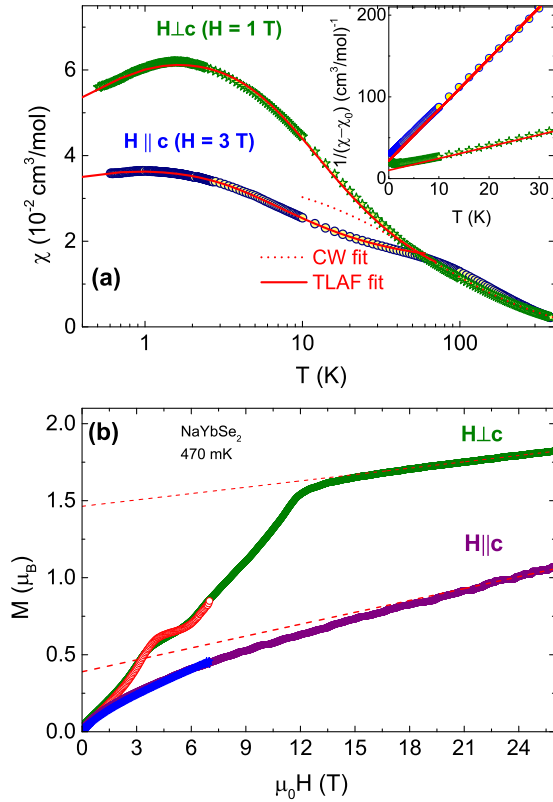


FIG. 3. (a) Magnetic susceptibilities (χ_{\parallel} and χ_{\perp}) of NaYbSe₂ single crystals. Red dotted and solid lines correspond to the high-temperature Curie-Weiss (CW) fit and TLAF fitting (see text), respectively. The inset shows the low-temperature inverse magnetic susceptibility after subtracting χ_{VV} along with the CW fit for both directions. (b) Isothermal magnetization $M(H)$ measured at 470 mK for both directions. Dashed lines represent the Van Vleck contribution (see text).

temperatures $T \geq 70$ K, $\chi(T)$ does not show a significant anisotropy and can be well described by

$$\chi(T)|_{T \geq 70 \text{ K}} = \chi^{\text{dia}} + \chi^{\text{VV}} + \frac{N_L \mu_0}{3} \frac{\mu_{\text{eff}}^2}{T - \Theta_{\text{CW}}}, \quad (1)$$

where χ^{dia} is a temperature-independent core diamagnetic contribution and χ^{VV} is the Van Vleck susceptibility in the limit $\mu_0 H \rightarrow 0$ neglecting the Curie term,

$$\chi^{\text{VV}} = N_L \mu_0 (g_j \mu_B)^2 \sum_n \sum_{m \neq n} M_{nm}^0 \frac{p_n^0 - p_m^0}{E_m^0 - E_n^0},$$

$$M_{nm}^0 := \sum_{\alpha \alpha'} |\langle n^0, \alpha | J_a | m^0, \alpha' \rangle|^2, \quad (2)$$

with the usual meaning of the constants; $g_j = 8/7$ denotes the Landé g factor for the Yb ion. Latin indices m and n indicate sums over the four CEF doublets with energies E_m^0 and E_n^0 ; Greek indices indicate the summation over the degenerate states within a doublet. The thermal population of a doublet n is given by $p_n^0 = \exp[-E_n^0/(k_B T)]/Z$, where $Z = 2 \sum_n \exp[-E_n^0/(k_B T)]$ denotes the partition function of the CEF doublets. The operator J_a is the component of the total

angular momentum operator in the direction of the applied field, and the bra and ket vectors denote the CEF eigenstates.

We obtain $\chi^{\text{dia}} + \chi^{\text{VV}} \approx 2 \times 10^{-4} \text{ cm}^3/\text{mol}$, a Weiss temperature $\Theta_{\text{CW}} = -66$ K, and an effective moment $\mu_{\text{eff}} = 4.5 \mu_B$, which are in good agreement with the literature [38]. The value of μ_{eff}/μ_B is close to the free-ion value $p = g_j \sqrt{j(j+1)} \approx 4.54$ for Yb³⁺ ($j = 7/2$).

A deviation from the Curie-Weiss (CW) behavior together with a large anisotropy is observed at low temperatures, indicating the evolution of a ground-state CEF doublet with small exchange couplings. $\chi_{\perp}(T)$ and $\chi_{\parallel}(T)$ did not show any signatures of magnetic LRO down to 0.5 K. Instead, $\chi_{\perp}(T)$ reveals a pronounced broad maximum centered around 2 K, a characteristic feature of strong magnetic short-range correlations associated with the low-dimensionality of the magnetic exchange. For $H \parallel c$, a similar broad maximum is observed at a slightly lower temperature.

Below 70 K, the magnetic properties of NaYbSe₂ are determined by the lowest Kramers doublet and can be described by an effective spin- $\frac{1}{2}$ model similar to NaYbO₂ and NaYbS₂ [39,40]. At low temperatures and finite applied magnetic fields, $\chi(T, H)$ has a sizable contribution from the Van Vleck susceptibility $\chi^{\text{VV}}(T, H)$ which arises from the excitations across the Zeeman-split CEF levels. In order to determine the χ^{VV} contribution experimentally, we have measured the isothermal high-field magnetization $M(H)$ at $T = 470$ mK for both the directions. As seen in Fig. 3(b), the in-plane magnetization (with $H \perp c$) has a kink at $\mu_0 H_{\perp}^s \approx 12$ T and increases linearly with higher fields. The linear behavior of $M_{\perp}(H)$ above about 13 T is due to the Van Vleck contribution, which can be estimated as $\chi_{\perp}^{\text{VV}} \approx 0.0137 \mu_B/T \approx 7.8 \times 10^{-4} \text{ cm}^3/\text{mol}$.

The Van Vleck contribution is found to be much larger for $H \parallel c$, but it is difficult to determine, as full saturation is not reached for $\mu_0 H \leq 22$ T. $M_{\parallel}(H)$ is expected to saturate at much higher fields compared to $M_{\perp}(H)$ (see below). A linear fitting above $\mu_0 H = 24$ T yields $\chi_{\parallel}^{\text{VV}} \approx 0.0257 \mu_B/T \approx 147 \times 10^{-4} \text{ cm}^3/\text{mol}$. The obtained saturation magnetizations $M_{\parallel}^s \approx 0.49 \mu_B$ and $M_{\perp}^s \approx 1.5 \mu_B$ are in good agreement with the expected values $M_{\perp, \parallel}^s = (1/2)g_{\perp, \parallel} \mu_B$ ($\sim 0.5 \mu_B$ and $\sim 1.5 \mu_B$ for $H \parallel c$ and $H \perp c$, respectively).

After subtracting χ^{VV} , $\chi(T)$ for $T \leq 30$ K could be fitted with a Curie-Weiss law [see inset of Fig. 3(a)], which yields $\Theta_{\text{CW}}^{\perp} \approx -7$ K, $\mu_{\text{eff}}^{\perp} \approx 2.43 \mu_B$ and $\Theta_{\text{CW}}^{\parallel} \approx -3.5$ K, $\mu_{\text{eff}}^{\parallel} \approx 1.1 \mu_B$ for the ab plane and c direction, respectively. The effective moments are in good agreement with $\mu_{\perp, \parallel} = g_{\perp, \parallel} \sqrt{S(S+1)} \mu_B$ for a pseudospin- $\frac{1}{2}$ ground state with the g values obtained from our ESR measurements ($2.7 \mu_B$ for $H \perp c$ and $0.9 \mu_B$ for $H \parallel c$).

2. Specific heat

Figure 4(a) shows the zero-field specific heat $C_p(T)$ of NaYbSe₂ along with that of the nonmagnetic reference NaLuO₂. First, it is evident that there is no magnetic LRO down to 50 mK in NaYbSe₂, which indeed points to a possible QSL ground state, similar to NaYbO₂ and NaYbS₂ [39,40]. Second, we observed a superposition of two broad maxima at low temperatures, $T_l \approx 1.1$ K and $T_h \approx 2.75$ K [Fig. 5(b)]. The zero-field $C_p(T)$ of NaYbSe₂ contains several

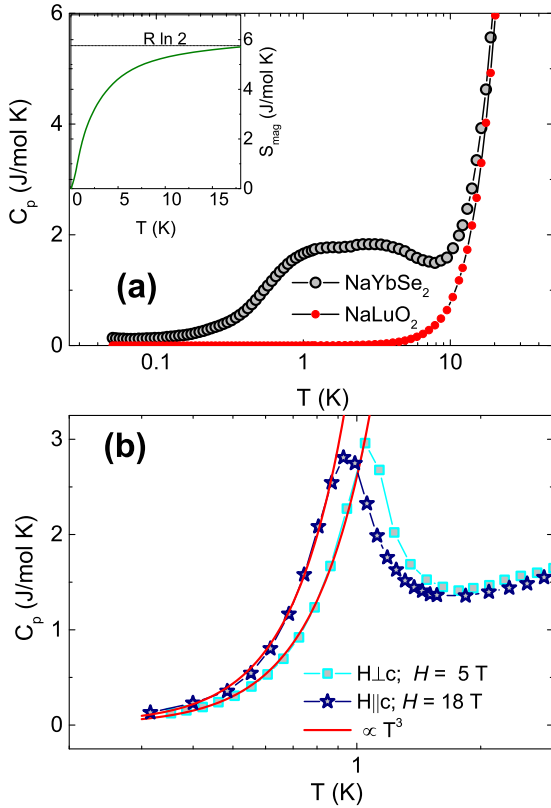


FIG. 4. (a) Zero-field specific heat of NaYbSe₂ and NaLuO₂. Inset: The calculated magnetic entropy as a function of temperature. The dotted line indicates the value of $R \ln 2$. (b) $C_p(T)$ data in the ordered states for $H \perp c$ (5 T) and $H \parallel c$ (18 T), together with a T^3 power law (see text).

contributions and can be written as $C_p(T) = C_{\text{nuc}}(T) + C_{\text{mag}}(T) + C_{\text{latt}}(T)$.

The magnetic contribution $C_{\text{mag}}(T)$ to the specific heat is obtained by correcting for the nuclear contribution $C_{\text{nuc}}(T)$ and subtracting the lattice contribution $C_{\text{latt}}(T)$, which is estimated from the specific heat of the isostructural reference compound NaLuO₂ after correcting for the mass difference. The upturn towards very low temperatures [Fig. 5(a)] results from the high-temperature part of a nuclear Schottky anomaly C_{nuc} of NaYbSe₂. This can be described by $C_{\text{nuc}} \propto \alpha/T^2$ in a first approach. As for many Yb systems, the nuclear Schottky contribution (mainly from ¹⁷¹Yb and ¹⁷³Yb) becomes sizable only below approximately 0.3 K [46]. The fit yields the coefficient $\alpha \simeq 2.2 \times 10^{-4}$ JK/mol, which seems to be a reasonable number for NaYbSe₂. Towards low temperatures, C_{mag} shows a nearly linear temperature dependence with a coefficient $\gamma = \frac{C_{\text{mag}}}{T} \simeq 1 \pm 0.1$ J/mol K², which clearly evidences a gapless QSL ground state. The calculated magnetic entropy $S_{\text{mag}}(T) (= \int_{0.05 \text{ K}}^T \frac{C_{\text{mag}}(T')}{T'} dT')$ is plotted in the inset of Fig. 4(a). At $T \simeq 15$ K, it reaches $R \ln 2$, as expected for an effective spin- $\frac{1}{2}$ state.

C. Field-induced effects

1. Magnetization studies

The isothermal magnetization [Fig. 3(b)] measured at $T = 0.47$ K for $H \perp c$ shows a clear plateau between 3 and 5 T

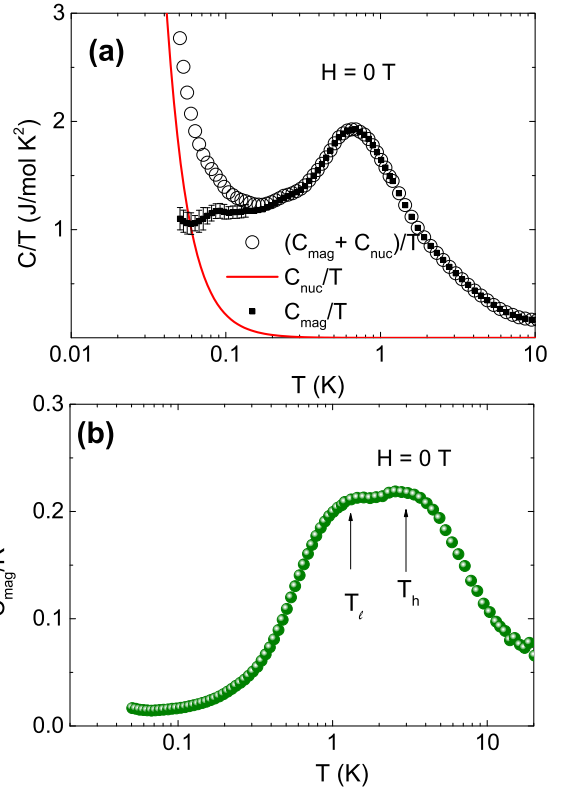


FIG. 5. (a) Temperature dependence of zero-field heat capacity divided by temperature, C_{mag}/T , for NaYbSe₂. The sharp upturn towards low temperatures due to the nuclear contribution is fitted with $C_{\text{nuc}} \propto \alpha/T^2$. (b) Temperature dependence of C_{mag}/R . T_l and T_h represent the low- T and high- T broad maxima at $T_l \simeq 1.1$ K and $T_h \simeq 2.75$ K.

at about one third of the saturation magnetization $M_{\perp}^s \simeq 1.5\mu_B$ when subtracting the Van Vleck contribution. The $M_s/3$ plateau is a manifestation of an uud bound-state spin arrangement, which is predicted by the mean-field theory [31]. Furthermore, the observation of the $M_s/3$ plateau for $H \perp c$ and the linear rise of the $M(H)$ curves for $H \parallel c$ are typical for an easy-plane type of magnetic anisotropy. Figure 6 shows more details on the $M(H)$ studies at different temperatures for $H \perp c$. In contrast, the linear behavior of $M(H)$ for $H \parallel c$ [Fig. 3(b)] suggests that the threefold rotational symmetry is not broken by the applied field; rather, a three-sublattice umbrellalike state emerges with the spins gradually canting out of the ab plane. Correspondingly, no plateau in $M(H)$ was observed for $H \parallel c$.

To learn more about the field-induced effects, we have measured $\chi(T)$ at higher fields for both $H \perp c$ and $H \parallel c$ [43]. Above 2 T, a kink in $\chi(T, H)$ was observed at low temperatures for $H \perp c$, which confirms the field-induced magnetic ordering in NaYbSe₂ above $\mu_0 H_{\perp} \simeq 2$ T. No such anomaly was observed for $H \parallel c$ up to $\mu_0 H_{\parallel} \simeq 7$ T.

2. Specific heat studies

$C_p(T)$ data measured at different applied fields, clearly evidencing the field-induced magnetic transitions in both directions, are shown in Fig. 7. The order manifests as a

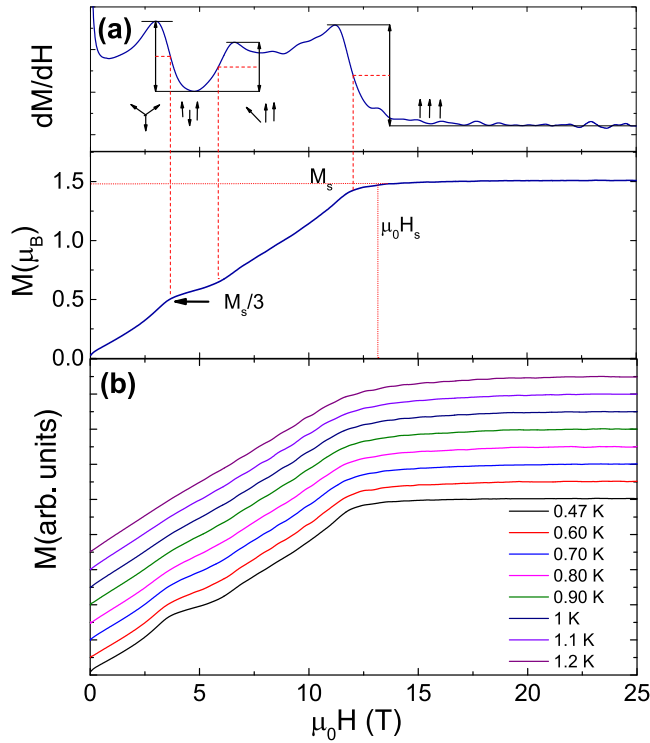


FIG. 6. (a) Analysis for the high-field magnetization isotherm for $H_{\perp}c$. The field boundaries for the uud phase and fully saturated phase are marked as red dashed lines. (b) Magnetization isotherms $M(H)$ measured at different temperatures for $H_{\perp}c$. Note that the curves are shifted by a constant offset in the magnetization.

peak that evolves from the low- T regime upon applying the magnetic fields. An external field of 2 T in the ab plane leads to a magnetic transition at $T_N \simeq 0.5$ K, whereas no such transition was observed for fields below 2 T. As shown in Fig. 7(a), this field-induced magnetic transition shifts towards higher temperatures with increasing magnetic field, reaching a maximum transition temperature at 5 T for $H \perp c$. A further increase of field results in a smooth decrease of T_N , which finally vanishes above $\mu_0 H_{\perp} \approx 9$ T. Therefore, a pronounced reentrant behavior of T_N is observed which includes the uud phase for $H \perp c$. No field-induced ordering was observed in this field range (2 to 8 T) for $H \parallel c$, whereas a field-induced transition with $T_N \simeq 0.5$ K appeared at $\mu_0 H_{\parallel} \approx 9$ T. The ordering temperature $T_N(H)$ follows a similar trend, i.e., a systematic initial increase of T_N up to 0.95 K at 16 T, and a shift towards lower temperatures with a further increase of field up to $\mu_0 H_{\parallel} = 21$ T. As seen in Fig. 4(b), $C_p(T)$ below T_N (at 5 T for $H \perp c$ and 18 T for $H \parallel c$) follows a well-defined T^3 behavior, which could be assigned to the emergence of three-dimensional magnons in a long-range-ordered antiferromagnetic state.

3. NMR measurements

We used ^{23}Na NMR measurements to further probe the field-induced magnetic ordering [43]. At higher temperatures, well-resolved ^{23}Na NMR spectra are observed, consisting of a sharp central line and two satellites, as expected for a spin- $\frac{3}{2}$ nucleus [43]. Upon decreasing the temperature, the NMR

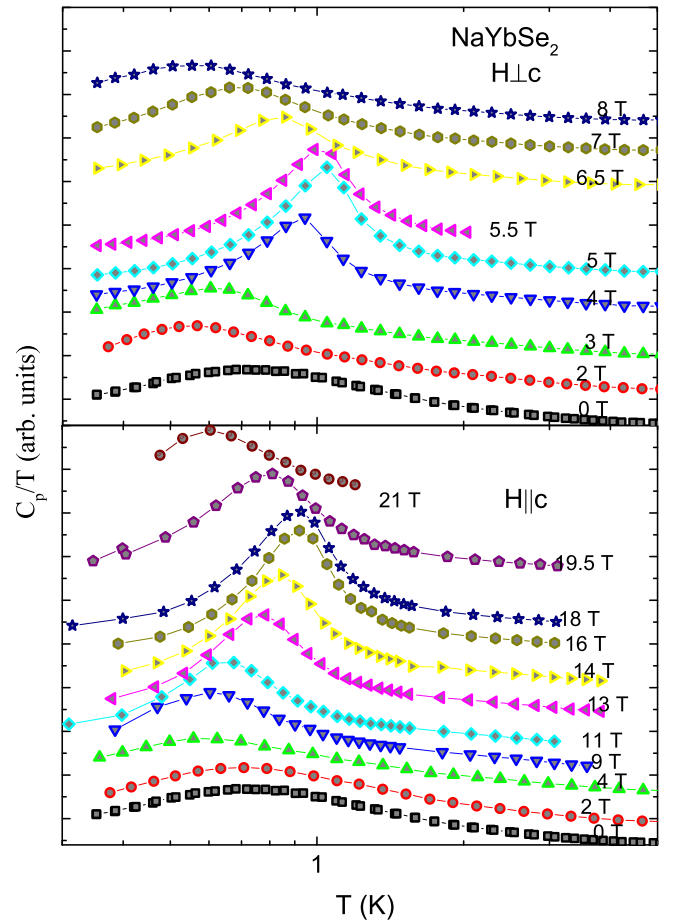


FIG. 7. Temperature-dependent specific heat of NaYbSe_2 , measured at different applied fields with orientations as indicated.

spectra are monotonously broadening and show an abrupt increase of inhomogeneous broadening below 1.1 K [43]. The sudden broadening of the NMR spectra below 1.1 K is due to the field-induced magnetic LRO in NaYbSe_2 , where the spectral width originates from the static internal field distribution at the ^{23}Na sites. The NMR spin-lattice relaxation rate $1/T_1$ probes the low-energy excitations, which clearly evidences the field-induced magnetic ordering at elevated fields. As seen in Fig. 8, $1/T_1$ measured for the fields in plane at $\mu_0 H_{\perp} \approx 5$ T and for the fields out of plane at $\mu_0 H_{\parallel} \approx 16$ T show a clear peak at around $T_N \simeq 1$ K corresponding to the field-induced magnetic LRO in both field directions.

IV. DISCUSSION

The eightfold degenerate $j = 7/2$ states of the Yb^{3+} ions are split into four Kramer's doublets. The ground-state doublet is well separated from the first excited doublet by an energy gap $\Delta/k_B \approx 160 \pm 30$ K. Therefore, the low-temperature properties can be well described by parametrizing the ground state with a pseudospin $\frac{1}{2}$ and corresponding effective g factors. The $R\bar{3}m$ space group symmetry allows for a NN exchange Hamiltonian, including the Zeeman coupling

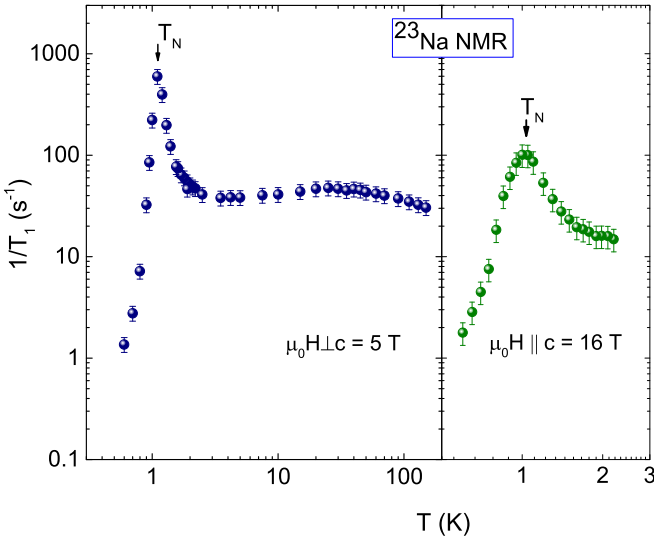


FIG. 8. ^{23}Na NMR spin-lattice relaxation rate in the magnetic ordered states for the field in plane at $\mu_0 H_{\perp c} = 5$ T and for the fields out of plane at $\mu_0 H_{\parallel c} = 16$ T.

to the external field $\mu_0 H$, of the general form

$$\begin{aligned} \mathcal{H} = & \sum_{\langle ij \rangle} \{ J_{\perp} (S_i^x S_j^x + S_i^y S_j^y) + J_z S_i^z S_j^z \\ & + \frac{1}{2} J_{\Delta} (e^{i\phi_{ij}} S_i^- S_j^- + e^{-i\phi_{ij}} S_i^+ S_j^+) \\ & + \frac{1}{2i} J_{yz} [e^{i\phi_{ij}} (S_i^z S_j^+ + S_i^+ S_j^z) \\ & - e^{-i\phi_{ij}} (S_i^z S_j^- + S_i^- S_j^z)] \} \\ & - \mu_0 \mu_B \sum_i [g_{\perp} (H_x S_i^x + H_y S_i^y) + g_{\parallel} H_z S_i^z], \\ \phi_{ij} = & \begin{cases} 0, & \vec{R}_i - \vec{R}_j = (\pm 1, 0), \\ \frac{2\pi}{3}, & \vec{R}_i - \vec{R}_j = \pm(-\frac{1}{2}, \frac{\sqrt{3}}{2}), \\ -\frac{2\pi}{3}, & \vec{R}_i - \vec{R}_j = \pm(-\frac{1}{2}, -\frac{\sqrt{3}}{2}), \end{cases} \end{aligned} \quad (3)$$

with $S_{\ell}^{\pm} = S_{\ell}^x \pm iS_{\ell}^y$. Here, $J_{\perp} = \frac{1}{2}(J_x + J_y)$ is the rotationally invariant exchange in the ab plane, and J_z is the exchange component parallel to the c axis [43]. The symmetry-allowed directional-dependent parts are $J_{\Delta} = \frac{1}{2}(J_x - J_y)$ and J_{yz} , with the latter describing the off-diagonal exchange coupling between spin components in the plane perpendicular to the bond direction $\vec{R}_i - \vec{R}_j$. We note that J_{Δ} and J_{yz} are the energies for a $|\Delta S| = 2$ and $|\Delta S| = 1$ excitation, respectively, and we expect these to be small compared to J_z and J_{\perp} . We note that in NaYbSe_2 , the Yb ions reside on a single highly symmetric site which precludes the antisymmetric (Dzyaloshinskii-Moriya) interaction for this compound [47].

Low-field thermodynamics

From the above spin Hamiltonian, the Curie-Weiss temperatures can be expressed as $\Theta_{\text{CW}}^{\perp} = -(3/2)J_{\perp}/k_B$ and

$\Theta_{\text{CW}}^{\parallel} = -(3/2)J_z/k_B$ for the field in the ab plane and parallel to the c axis, respectively [33]. Our low-temperature CW analysis ($\Theta_{\text{CW}}^{\perp} \simeq -7$ K and $\Theta_{\text{CW}}^{\parallel} \simeq -3.5$) yields $J_{\perp}/k_B \simeq 4.7$ K and $J_z/k_B \simeq 2.33$ K, which indicates a less anisotropic exchange compared to NaYbS_2 [39].

It is worth noting that the presence of broad maxima in the susceptibility and specific heat is consistent with a quasi-two-dimensional scenario. For an isotropic $S = 1/2$ TLAf with exchange J , such a broad maximum of $\chi(T)$ is expected at $k_B T_{\text{max}}^{\chi} \lesssim J$ [33]. Below 70 K, the overall behavior of both $\chi_{\perp}(T)$ and $\chi_{\parallel}(T)$ could be well described by the following Padé approximation to the high-temperature series expansion given by [48]:

$$\chi(T) = \frac{N_L \mu_0 g^2 \mu_B^2}{4k_B T} \frac{1 + b_1 x + \dots + b_6 x^6}{1 + c_1 x + \dots + c_7 x^7} \Big|_{x=J/(4k_B T)}. \quad (4)$$

The coefficients $\{b_i\}$ and $\{c_i\}$ are listed in Ref. [49].

As seen in Fig. 3(a), the $\chi(T)$ data below 70 K can be fitted well by Eq. (4). Above 70 K, a deviation was observed, which is expected due to the thermal population of the energetically higher CEF doublets. The obtained fitting parameters, $g_{\perp} \simeq 3.0(2)$, $J_{\perp}/k_B \simeq 4.5(3)$ K and $g_{\parallel} \simeq 1.2(1)$, $J_z/k_B \simeq 2.4(3)$ K, are in good agreement with our ESR g factors ($g_{\perp} \approx 3.1$ and $g_{\parallel} \approx 1.2$) and the exchange couplings ($J_{\perp}/k_B \approx 4.7$ K and $J_z/k_B \approx 2.33$ K) derived from the low-temperature Curie-Weiss analysis. From Eq. (3), the expression for the saturation field can be derived as $\mu_0 H_{\perp}^{\text{sat}} = \frac{9S J_{\perp} k_B}{\mu_B g_{\perp}}$ and $\mu_0 H_{\parallel}^{\text{sat}} = \frac{3S(2J_z + J_{\perp})k_B}{\mu_B g_{\parallel}}$ for the field in the ab plane and parallel to the c axis, respectively [43]. The calculated values $\mu_0 H_{\perp}^{\text{sat}} \simeq 10.2$ T and $\mu_0 H_{\parallel}^{\text{sat}} \simeq 21$ T are slightly below the observed values of 12 and 25 T, respectively. This might indicate the presence of antiferromagnetic next-NN interactions in NaYbSe_2 .

Moreover, the zero-field $C_{\text{mag}}(T)$ shows a superposition of two broad peaks at around 1.1 and 2.75 K [see Fig. 5(b)]. This is rather unusual for a 2D nearest-neighbor TLAf, for which one would expect only a single maximum at $k_B T \approx 0.55J_{2D}$ [48]. However, such double broad maxima in $C_p(T)$ are predicted for 2D triangular and kagome lattice antiferromagnets with a fully frustrated disordered ground state [50,51]. A similar feature was experimentally observed in the recently reported 2D TLAf compound $\text{Ba}_8\text{CoNb}_6\text{O}_{24}$ [52,53]. Recent numerical simulations based on an exponential tensor renormalization group method reveal two crossover temperature scales in $C_{\text{mag}}(T)$ for a spin- $\frac{1}{2}$ TLAf, at $T_l/J \simeq 0.2$ and $T_h/J \simeq 0.55$ [54]. The anticipated positions of the maxima with $J_{\perp} \simeq 4.7$ K closely match our experimental data. The absolute values of the maxima are very sensitive to the degree of magnetic frustration. Broad maxima with $C_{\text{mag}}^{\text{max}} \simeq 0.44R$ and $0.35R$ are expected for a nonfrustrated square lattice and spin chain, respectively, where R is the gas constant [55,56]. In the case of a highly frustrated triangular lattice, $C_{\text{mag}}^{\text{max}}$ is expected to be much smaller ($0.22R$) [48,57]. Our value of $C_{\text{mag}}^{\text{max}} \simeq 0.218R$ matches well the one expected for a TLAf [see Fig. 5(b)].

The exchange anisotropy, which is common for an effective spin- $\frac{1}{2}$ ground-state doublet of Yb^{3+} , is estimated as $J_z/J_{\perp} \simeq 0.5$ for NaYbSe_2 . In TLAfs with isotropic exchange as well as with easy-plane anisotropy, the ground state is a 120° coplanar state. In contrast, multiple ordered phases (low-temperature

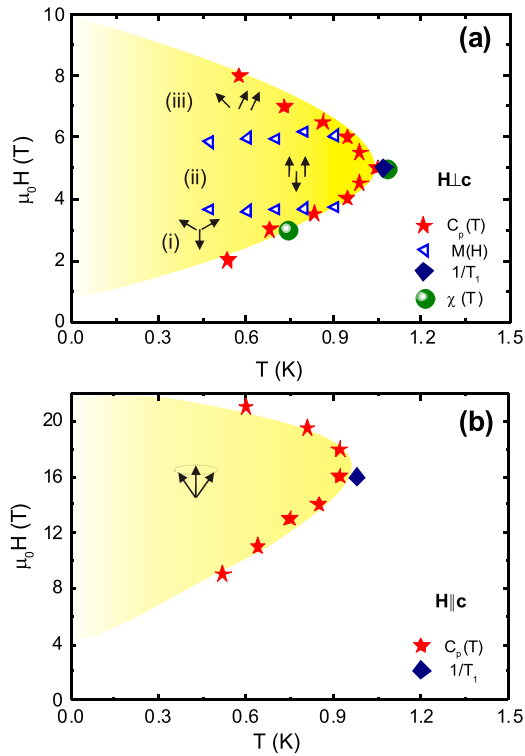


FIG. 9. Field-temperature phase diagram of NaYbSe₂ for $H \perp c$ and $H \parallel c$.

120° state and an intermediate-temperature collinear state) are predicted for easy-axis-type anisotropy [58–62]. NaYbSe₂ does not show any magnetic LRO at zero fields. Instead, we observed a gapless and strongly fluctuating state. Only towards higher applied fields is the magnetic order induced and stabilized with increasing field strength. Recently, Zhu *et al.* constructed a four-dimensional extension of the phase diagram for the anisotropic bond-dependent XXZ model with next-NN coupling J_2 , which can host a spin-liquid phase and is continuously connected to a spin-liquid phase of the isotropic J_1 - J_2 model [63]. In contrast to the impact of next-NN couplings on the ground state, it should be noted that the off-diagonal terms in the bond exchange matrices can influence the ground state and yield strong zero-field fluctuations. So far, we do not have any estimate for these higher exchange terms. In the case of YbMgGaO₄, these interactions are reported to be rather small [64].

Figures 9(a) and 9(b) represent the H - T phase diagrams for both the $H \perp c$ and $H \parallel c$ directions, respectively, constructed from the field-dependent $C_p(T)$ (Fig. 7) and temperature-dependent $M(H)$ (Fig. 6) measurements. For $H \perp c$, we may assign different spin configurations: In the low-field regime (below 1 T), a highly fluctuating QSL-like phase with persistent gapless excitations was observed instead of the 120° ordered phase expected for a TLAF with easy-plane anisotropy. In region (i), above approximately 1 T, an oblique 120° spin structure (Y -coplanar) structure may be stabilized by the application of a moderate external field along the ab plane. Upon increasing the field, the transition from Y coplanar to the collinear uud phase appears at about ≈ 3 T [region (ii)], which manifests as the $M_{\perp}^s/3$ plateau in $M(H)$ [see Fig. 3(b)]. With

further increasing field, a 2:1 coplanar magnetic phase might appear above $\mu_0 H_{\perp} \approx 6$ T [region (iii)], before reaching full saturation at $\mu_0 H_{\perp}^s \approx 12$ T. It should be mentioned that the phase boundaries from the specific heat represent second-order phase transitions, whereas the open symbols obtained from $M(H)$ represent crossover lines between the different spin textures.

A magnetic field parallel to the c axis does not break the threefold rotational symmetry of the crystal. Therefore, a single magnetically ordered umbrella-shaped three-sublattice phase is induced, here at fields $\mu_0 H_{\parallel} \gtrsim 9$ T, substantially higher than the in-plane field. In concordance with this, the saturation field at low temperatures exceeds $\mu_0 H_{\parallel} \simeq 21$ T, where T_N is still finite. Single-crystal neutron diffraction measurements under external magnetic fields will be necessary to determine the magnetic structure in more detail.

The overall shape of the phase diagram is in good agreement with results from classical Monte Carlo simulations [65], apart from the low-field disordered regime. Similar H - T phase diagrams for $H \perp c$ and $H \parallel c$ are also reported for the effective spin- $\frac{1}{2}$ TLAF Ba₃CoSb₂O₉ [66,67]. In contrast to these, the field-induced magnetic transitions are highly anisotropic in NaYbSe₂. Moreover, the H - T phase diagram contains both a QSL phase and a full range of ordered phases for a prototypical $S = 1/2$ TLAF, again different from Ba₃CoSb₂O₉ or any other TLAFs. In this sense, NaYbSe₂ provides a unique opportunity to study the low-temperature properties of pseudospin $S = 1/2$ triangular-lattice antiferromagnets.

V. CONCLUSION

In conclusion, we have synthesized and investigated high-quality single crystals of NaYbSe₂, a Yb-based triangular-lattice QSL candidate without any inherent disorder. The ground-state doublet is well separated from the first excited-state doublet, inducing a (pseudo)spin- $\frac{1}{2}$ ground state, as confirmed by ESR measurements and a low-temperature entropy analysis. Zero-field measurements confirm the absence of magnetic LRO down to 50 mK, suggesting a gapless QSL ground state. Strong bond frustration introduces a melting of the predicted 120° order at zero fields. The QSL ground state is found to be unstable against applied magnetic fields. A clear $\frac{M_s}{3}$ magnetization plateau, associated with an up-up-down spin configuration, was observed for the $H \perp c$ direction. The reentrant behavior of T_N , originating from the thermal and quantum spin fluctuations, is observed for both directions. The obtained H - T phase diagram is highly anisotropic and includes different quantum phases expected for a triangular-lattice antiferromagnet, which classifies NaYbSe₂ as a unique model system and opens up future theoretical and experimental studies.

Note added. Recently, we became aware of Refs. [68,69] where, another family of Yb dichalcogenide delafossites was investigated experimentally.

ACKNOWLEDGMENTS

We thank A. Mackenzie, H. Rosner, C. Geibel, L. Hozoi, J. Rau, A. A. Tsirlin, and A. L. Chernyshev for fruitful

discussions. We thank C. Klausnitzer and H. Rave for technical support. We acknowledge the support from the Deutsche Forschungsgemeinschaft (DFG) through SFB 1143 and the Würzburg-Dresden Cluster of Excellence on Complexity and

Topology in Quantum Matter - ct.qmat (EXC 2147, project ID 39085490), as well as from the HLD at HZDR, a member of the European Magnetic Field Laboratory. A.M.S. thanks SA-NRF (105702) for financial assistance.

-
- [1] L. Balents, Spin liquids in frustrated magnets, *Nature (London)* **464**, 199 (2010).
- [2] Y. Zhou, K. Kanoda, and T.-K. Ng, Quantum spin liquid states, *Rev. Mod. Phys.* **89**, 025003 (2017).
- [3] J. Wen, S. L. Yu, S. Li, W. Yu, and J.-X. Li, Experimental identification of quantum spin liquids, *npj Quantum Mater.* **4**, 12 (2019).
- [4] P. W. Anderson, Resonating valence bonds: A new kind of insulator? *Mater. Res. Bull.* **8**, 153 (1973).
- [5] B. Bernu, P. Lecheminant, C. Lhuillier, and L. Pierre, Exact spectra, spin susceptibilities, and order parameter of the quantum Heisenberg antiferromagnet on the triangular lattice, *Phys. Rev. B* **50**, 10048 (1994).
- [6] L. Capriotti, A. E. Trumper, and S. Sorella, Long-Range Néel Order in the Triangular Heisenberg Model, *Phys. Rev. Lett.* **82**, 3899 (1999).
- [7] Z. Zhu and S. R. White, Spin liquid phase of the $s = \frac{1}{2}J_1 - J_2$ Heisenberg model on the triangular lattice, *Phys. Rev. B* **92**, 041105(R) (2015).
- [8] Y. Iqbal, W.-J. Hu, R. Thomale, D. Poilblanc, and F. Becca, Spin liquid nature in the Heisenberg $J_1 - J_2$ triangular antiferromagnet, *Phys. Rev. B* **93**, 144411 (2016).
- [9] S. Yunoki and S. Sorella, Two spin liquid phases in the spatially anisotropic triangular Heisenberg model, *Phys. Rev. B* **74**, 014408 (2006).
- [10] T. Shimokawa, K. Watanabe, and H. Kawamura, Static and dynamical spin correlations of the $s = \frac{1}{2}$ random-bond antiferromagnetic Heisenberg model on the triangular and kagome lattices, *Phys. Rev. B* **92**, 134407 (2015).
- [11] Y. Shimizu, K. Miyagawa, K. Kanoda, M. Maesato, and G. Saito, Spin Liquid State in an Organic Mott Insulator with a Triangular Lattice, *Phys. Rev. Lett.* **91**, 107001 (2003).
- [12] S. Yamashita, Y. Nakazawa, M. Oguni, Y. Oshima, H. Nojiri, Y. Shimizu, K. Miyagawa, and K. Kanoda, Thermodynamic properties of a spin-1/2 spin-liquid state in a κ -type organic salt, *Nat. Phys.* **4**, 459 (2008).
- [13] M. Yamashita, N. Nakata, Y. Senshu, M. Nagata, H. M. Yamamoto, R. Kato, T. Shibauchi, and Y. Matsuda, Highly mobile gapless excitations in a two-dimensional candidate quantum spin liquid, *Science* **328**, 1246 (2010).
- [14] T. Isono, T. Terashima, K. Miyagawa, K. Kanoda, and S. Uji, Quantum criticality in an organic spin-liquid insulator κ -(BEDT-TTF)₂Cu₂(CN)₃, *Nat. Commun.* **7**, 13494 (2016).
- [15] S. Yamashita, T. Yamamoto, Y. Nakazawa, M. Tamura, and R. Kato, Gapless spin liquid of an organic triangular compound evidenced by thermodynamic measurements, *Nat. Commun.* **2**, 275 (2011).
- [16] T. Itou, A. Oyamada, S. Maegawa, M. Tamura, and R. Kato, Quantum spin liquid in the spin- $\frac{1}{2}$ triangular antiferromagnet EtMe₃Sb[Pd(dmit)₂]₂, *Phys. Rev. B* **77**, 104413 (2008).
- [17] H. D. Zhou, E. S. Choi, G. Li, L. Balicas, C. R. Wiebe, Y. Qiu, J. R. D. Copley, and J. S. Gardner, Spin Liquid State in the $S = 1/2$ Triangular Lattice Ba₃CuSb₂O₉, *Phys. Rev. Lett.* **106**, 147204 (2011).
- [18] J. G. Rau and M. J. P. Gingras, Frustration and anisotropic exchange in ytterbium magnets with edge-shared octahedra, *Phys. Rev. B* **98**, 054408 (2018).
- [19] P. A. Maksimov, Z. Zhu, S. R. White, and A. L. Chernyshev, Anisotropic-Exchange Magnets on a Triangular Lattice: Spin Waves, Accidental Degeneracies, and Dual Spin Liquids, *Phys. Rev. X* **9**, 021017 (2019).
- [20] G. Chen, L. Balents, and A. P. Schnyder, Spin-Orbital Singlet and Quantum Critical Point on the Diamond Lattice: FeSc₂S₄, *Phys. Rev. Lett.* **102**, 096406 (2009).
- [21] G. Jackeli and G. Khaliullin, Mott Insulators in the Strong Spin-Orbit Coupling Limit: From Heisenberg to a Quantum Compass and Kitaev Models, *Phys. Rev. Lett.* **102**, 017205 (2009).
- [22] H. Ishizuka and L. Balents, Magnetism in $S = \frac{1}{2}$ double perovskites with strong spin-orbit interactions, *Phys. Rev. B* **90**, 184422 (2014).
- [23] L. Lu, M. Song, W. Liu, A. P. Reyes, P. Kuhns, H. O. Lee, I. R. Fisher, and V. F. Mitrović, Magnetism and local symmetry breaking in a Mott insulator with strong spin orbit interactions, *Nat. Commun.* **8**, 14407 (2017).
- [24] Y. Li, H. Liao, Z. Zhang, S. Li, F. Jin, L. Ling, L. Zhang, Y. Zou, L. Pi, Z. Yang, J. Wang, Z. Wu, and Q. Zhang, Gapless quantum spin liquid ground state in the two-dimensional spin-1/2 triangular antiferromagnet YbMgGaO₄, *Sci. Rep.* **5**, 16419 (2015).
- [25] Y. Li, G. Chen, W. Tong, L. Pi, J. Liu, Z. Yang, X. Wang, and Q. Zhang, Rare-Earth Triangular Lattice Spin Liquid: A Single-Crystal Study of YbMgGaO₄, *Phys. Rev. Lett.* **115**, 167203 (2015).
- [26] Y. Shen, Y.-D. Li, H. Wo, Y. Li, S. Shen, B. Pan, Q. Wang, H. C. Walker, P. Steffens, M. Boehm, Y. Hao, D. L. Quintero-Castro, L. W. Harriger, M. D. Frontzek, L. Hao, S. Meng, Q. Zhang, G. Chen, and J. Zhao, Evidence for a spinon Fermi surface in a triangular-lattice quantum-spin-liquid candidate, *Nature (London)* **540**, 559 (2016).
- [27] J. A. M. Paddison, M. Daum, Z. Dun, G. Ehlers, Y. Liu, M. B. Stone, H. Zhou, and M. Mourigal, Continuous excitations of the triangular-lattice quantum spin liquid YbMgGaO₄, *Nat. Phys.* **13**, 117 (2017).
- [28] Y. Xu, J. Zhang, Y. S. Li, Y. J. Yu, X. C. Hong, Q. M. Zhang, and S. Y. Li, Absence of Magnetic Thermal Conductivity in the Quantum Spin-Liquid Candidate YbMgGaO₄, *Phys. Rev. Lett.* **117**, 267202 (2016).
- [29] Y. Li, D. Adroja, R. I. Bewley, D. Voneshen, A. A. Tsirlin, P. Gegenwart, and Q. Zhang, Crystalline Electric-Field Randomness in the Triangular Lattice Spin-Liquid YbMgGaO₄, *Phys. Rev. Lett.* **118**, 107202 (2017).

- [30] Z. Zhu, P. A. Maksimov, S. R. White, and A. L. Chernyshev, Disorder-Induced Mimicry of a Spin Liquid in YbMgGaO_4 , *Phys. Rev. Lett.* **119**, 157201 (2017).
- [31] A. V. Chubokov and D. I. Golosov, Quantum theory of an antiferromagnet on a triangular lattice in a magnetic field, *J. Phys.: Condens. Matter* **3**, 69 (1991).
- [32] H. Kawamura and S. Miyashita, Phase transition of the Heisenberg antiferromagnet on the triangular lattice in a magnetic field, *J. Phys. Soc. Jpn.* **54**, 4530 (1985).
- [33] B. Schmidt and P. Thalmeier, Frustrated two dimensional quantum magnets, *Phys. Rep.* **703**, 1 (2017).
- [34] T. Ono, H. Tanaka, H. Aruga Katori, F. Ishikawa, H. Mitamura, and T. Goto, Magnetization plateau in the frustrated quantum spin system Cs_2CuBr_4 , *Phys. Rev. B* **67**, 104431 (2003).
- [35] J. Alicea, A. V. Chubokov, and O. A. Starykh, Quantum Stabilization of the 1/3-Magnetization Plateau in Cs_2CuBr_4 , *Phys. Rev. Lett.* **102**, 137201 (2009).
- [36] N. A. Fortune, S. T. Hannahs, Y. Yoshida, T. E. Sherline, T. Ono, H. Tanaka, and Y. Takano, Cascade of Magnetic-Field-Induced Quantum Phase Transitions in a Spin- $\frac{1}{2}$ Triangular-Lattice Antiferromagnet, *Phys. Rev. Lett.* **102**, 257201 (2009).
- [37] T. Susuki, N. Kurita, T. Tanaka, H. Nojiri, A. Matsuo, K. Kindo, and H. Tanaka, Magnetization Process and Collective Excitations in the $S=1/2$ Triangular-Lattice Heisenberg Antiferromagnet $\text{Ba}_3\text{CoSb}_2\text{O}_9$, *Phys. Rev. Lett.* **110**, 267201 (2013).
- [38] W. Liu, Z. Zhang, J. Ji, Y. Liu, J. Li, X. Wang, H. Lei, G. Chen, and Q. Zhang, Rare-earth chalcogenides: A large family of triangular lattice spin liquid candidates, *Chin. Phys. Lett.* **35**, 117501 (2018).
- [39] M. Baenitz, Ph. Schlender, J. Sichelschmidt, Y. A. Onykieenko, Z. Zangeneh, K. M. Ranjith, R. Sarkar, L. Hozoi, H. C. Walker, J.-C. Orain, H. Yasuoka, J. van den Brink, H. H. Klauss, D. S. Inosov, and Th. Doert, NaYbS_2 : A planar spin- $\frac{1}{2}$ triangular-lattice magnet and putative spin liquid, *Phys. Rev. B* **98**, 220409(R) (2018).
- [40] K. M. Ranjith, D. Dmytriieva, S. Khim, J. Sichelschmidt, S. Luther, D. Ehlers, H. Yasuoka, J. Wosnitza, A. A. Tsirlin, H. Kühne, and M. Baenitz, Field-induced instability of the quantum spin liquid ground state in the $J_{\text{eff}} = \frac{1}{2}$ triangular-lattice compound NaYbO_2 , *Phys. Rev. B* **99**, 180401(R) (2019).
- [41] L. Ding, P. Manuel, S. Bachus, F. Grubler, P. Gegenwart, J. Singleton, R. D. Johnson, H. C. Walker, D. T. Adroja, A. D. Hillier, and A. A. Tsirlin, Gapless spin-liquid state in the structurally disorder-free triangular antiferromagnet NaYbO_2 , *Phys. Rev. B* **100**, 144432 (2019).
- [42] M. M. Bordelon, E. Kenney, C. Liu, T. Hogan, L. Posthuma, M. Kavand, Y. Lyu, M. Sherwin, N. P. Butch, C. Brown, M. J. Graf, L. Balents, and S. D. Wilson, Field-tunable quantum disordered ground state in the triangular-lattice antiferromagnet NaYbO_2 , *Nat. Phys.* **15**, 1058 (2019).
- [43] See Supplemental Material at <http://link.aps.org/supplemental/10.1103/PhysRevB.100.224417> for the details of theoretical analysis and additional/supporting measurement details and results, which includes Refs. [18,25,40,47,63,70–73].
- [44] J. Sichelschmidt, Ph. Schlender, B. Schmidt, M. Baenitz, and Th. Doert, Electron spin resonance on the spin-1/2 triangular magnet NaYbS_2 , *J. Phys.: Condens. Matter* **31**, 205601 (2019).
- [45] J. Sichelschmidt, B. Schmidt, Ph. Schlender, S. Khim, Th. Doert, and M. Baenitz, Effective spin- $\frac{1}{2}$ moments on a Yb^{3+} triangular lattice: An ESR study, [arXiv:1912.01868](https://arxiv.org/abs/1912.01868) [JPS Conf. Proc. (to be published)].
- [46] A. Steppke, M. Brando, N. Oeschler, C. Krellner, C. Geibel, and F. Steglich, Nuclear contribution to the specific heat of $\text{Yb}(\text{Rh}_{0.93}\text{Co}_{0.07})_2\text{Si}_2$, *Phys. Status Solidi B* **247**, 737 (2010).
- [47] T. Moriya, Anisotropic superexchange interaction and weak ferromagnetism, *Phys. Rev.* **120**, 91 (1960).
- [48] N. Elstner, R. R. P. Singh, and A. P. Young, Finite Temperature Properties of the Spin-1/2 Heisenberg Antiferromagnet on the Triangular Lattice, *Phys. Rev. Lett.* **71**, 1629 (1993).
- [49] M. Tamura and R. Kato, Magnetic susceptibility of β' - $[\text{Pd}(\text{dmit})_2]$ salts (dmit = 1, 3-dithiol-2-thione-4, 5-dithiolate, C_3S_5): Evidence for frustration in spin-1/2 Heisenberg antiferromagnets on a triangular lattice, *J. Phys.: Condens. Matter* **14**, L729 (2002).
- [50] K. Ishida, M. Morishita, K. Yawata, and H. Fukuyama, Low Temperature Heat-Capacity Anomalies in Two-Dimensional Solid ^3He , *Phys. Rev. Lett.* **79**, 3451 (1997).
- [51] V. Elser, Nuclear Antiferromagnetism in a Registered ^3He Solid, *Phys. Rev. Lett.* **62**, 2405 (1989).
- [52] R. Rawl, L. Ge, H. Agrawal, Y. Kamiya, C. R. Dela Cruz, N. P. Butch, X. F. Sun, M. Lee, E. S. Choi, J. Oitmaa, C. D. Batista, M. Mourigal, H. D. Zhou, and J. Ma, $\text{Ba}_8\text{CoNb}_6\text{O}_{24}$: A spin- $\frac{1}{2}$ triangular-lattice Heisenberg antiferromagnet in the two-dimensional limit, *Phys. Rev. B* **95**, 060412(R) (2017).
- [53] Y. Cui, J. Dai, P. Zhou, P. S. Wang, T. R. Li, W. H. Song, J. C. Wang, L. Ma, Z. Zhang, S. Y. Li, G. M. Luke, B. Normand, T. Xiang, and W. Yu, Mermin-Wagner physics, (H, T) phase diagram, and candidate quantum spin-liquid phase in the spin- $\frac{1}{2}$ triangular-lattice antiferromagnet $\text{Ba}_8\text{CoNb}_6\text{O}_{24}$, *Phys. Rev. Mater.* **2**, 044403 (2018).
- [54] L. Chen, D.-W. Qu, H. Li, B.-B. Chen, S.-S. Gong, J. von Delft, A. Weichselbaum, and W. Li, Two-temperature scales in the triangular-lattice Heisenberg antiferromagnet, *Phys. Rev. B* **99**, 140404(R) (2019).
- [55] D. C. Johnston, R. K. Kremer, M. Troyer, X. Wang, A. Klümper, S. L. Bud'ko, A. F. Panchula, and P. C. Canfield, Thermodynamics of spin $S = 1/2$ antiferromagnetic uniform and alternating-exchange Heisenberg chains, *Phys. Rev. B* **61**, 9558 (2000).
- [56] M. Hofmann, T. Lorenz, K. Berggold, M. Grüninger, A. Freimuth, G. S. Uhrig, and E. Brück, Evidence for a large magnetic heat current in insulating layered cuprates, *Phys. Rev. B* **67**, 184502 (2003).
- [57] B. Bernu and G. Misguich, Specific heat and high-temperature series of lattice models: Interpolation scheme and examples on quantum spin systems in one and two dimensions, *Phys. Rev. B* **63**, 134409 (2001).
- [58] S. Miyashita, Magnetic properties of Ising-like Heisenberg antiferromagnets on the triangular lattice, *J. Phys. Soc. Jpn.* **55**, 3605 (1986).
- [59] F. Matsubara, Magnetic ordering in a hexagonal antiferromagnet, *J. Phys. Soc. Jpn.* **51**, 2424 (1982).
- [60] P.-É. Melchy and M. E. Zhitomirsky, Interplay of anisotropy and frustration: Triple transitions in a triangular-lattice antiferromagnet, *Phys. Rev. B* **80**, 064411 (2009).
- [61] K. M. Ranjith, R. Nath, M. Majumder, D. Kasinathan, M. Skoulatos, L. Keller, Y. Skourski, M. Baenitz, and A. A. Tsirlin,

- Commensurate and incommensurate magnetic order in spin-1 chains stacked on the triangular lattice in $\text{Li}_2\text{NiW}_2\text{O}_8$, [Phys. Rev. B **94**, 014415 \(2016\)](#).
- [62] K. M. Ranjith, K. Brinda, U. Arjun, N. G. Hegde, and R. Nath, Double phase transition in the triangular antiferromagnet $\text{Ba}_3\text{CoTa}_2\text{O}_9$, [J. Phys. Condens. Matter **29**, 115804 \(2017\)](#).
- [63] Z. Zhu, P. A. Maksimov, Steven R. White, and A. L. Chernyshev, Topography of Spin Liquids on a Triangular Lattice, [Phys. Rev. Lett. **120**, 207203 \(2018\)](#).
- [64] X. Zhang, F. Mahmood, M. Daum, Z. Dun, J. A. M. Paddison, N. J. Laurita, T. Hong, H. Zhou, N. P. Armitage, and M. Mourigal, Hierarchy of Exchange Interactions in the Triangular-Lattice Spin Liquid YbMgGaO_4 , [Phys. Rev. X **8**, 031001 \(2018\)](#).
- [65] L. Seabra, T. Momoi, P. Sindzingre, and N. Shannon, Phase diagram of the classical Heisenberg antiferromagnet on a triangular lattice in an applied magnetic field, [Phys. Rev. B **84**, 214418 \(2011\)](#).
- [66] G. Quirion, M. Lapointe-Major, M. Poirier, J. A. Quilliam, Z. L. Dun, and H. D. Zhou, Magnetic phase diagram of $\text{Ba}_3\text{CoSb}_2\text{O}_9$ as determined by ultrasound velocity measurements, [Phys. Rev. B **92**, 014414 \(2015\)](#).
- [67] G. Koutroulakis, T. Zhou, Y. Kamiya, J. D. Thompson, H. D. Zhou, C. D. Batista, and S. E. Brown, Quantum phase diagram of the $S = \frac{1}{2}$ triangular-lattice antiferromagnet $\text{Ba}_3\text{CoSb}_2\text{O}_9$, [Phys. Rev. B **91**, 024410 \(2015\)](#).
- [68] J. Xing, L. D. Sanjeeewa, J. Kim, G. R. Stewart, M.-H. Du, F. A. Reboredo, R. Custelcean, and A. S. Sefat, Crystal synthesis and frustrated magnetism in triangular lattice CsRESe_2 (RE= La-Lu): Quantum spin liquid candidates CsCeSe_2 and CsYbSe_2 , [ACS Mater. Lett. **2**, 71 \(2020\)](#).
- [69] J. Xing, L. D. Sanjeeewa, J. Kim, G. R. Stewart, A. Podlesnyak, and A. S. Sefat, Field-induced magnetic transition and spin fluctuation in quantum spin liquid candidate CsYbSe_2 , [Phys. Rev. B **100**, 220407\(R\) \(2019\)](#).
- [70] P. Fulde, Crystal fields, in *Handbook on the Physics and Chemistry of Rare Earths* (Elsevier, North-Holland Publishing Company, 1979), Vol. 2, pp. 295.
- [71] T. Itou, A. Oyamada, S. Maegawa, and R. Kato, Instability of a quantum spin liquid in an organic triangular-lattice antiferromagnet, [Nat. Phys. **6**, 673 \(2010\)](#).
- [72] A. C. Shockley, F. Bert, J. C. Orain, Y. Okamoto, and P. Mendels, Frozen State and Spin Liquid Physics in $\text{Na}_4\text{Ir}_3\text{O}_8$: An NMR study, [Phys. Rev. Lett. **115**, 047201 \(2015\)](#).
- [73] K. M. Ranjith, C. Klein, A. A. Tsirlin, H. Rosner, C. Krellner, and M. Baenitz, Magnetic resonance as a local probe for kagomé magnetism in barlowite $\text{Cu}_4(\text{OH})_6\text{FBr}$, [Sci. Rep. **8**, 10851 \(2018\)](#).